Effect of the Initial Vortex Structure on Intensity Change during Eyewall

Replacement Cycle of Tropical Cyclones: A Numerical Study

3	Xinwei Yang ^{1,2} , Yuqing Wang ³ , Hui Wang ² , Jing Xu ^{2,4} , and Ruifen Zhan ⁵ ,
4	¹ University of Chinese Academy of Sciences, Beijing, China
5	² State Key Laboratory of Severe Weather, Chinese Academy of Meteorological Sciences,
6	China Meteorological Administration, Beijing, China
7	³ Department of Atmospheric Sciences and International Pacific Research Center, School of
8	Earth and Ocean Science and Technology, University of Hawaii at Manoa, Honolulu, HI
9	96822, UAS
10	⁴ Qingdao Joint Institute of Marine Meteorology, Chinese Academy of Meteorological
11	Sciences, China Meteorological Administration, Beijing, China
12	⁵ Department of Atmospheric and Oceanic Sciences & Institute of Atmospheric Sciences,
13	Fudan University, Shanghai, China
14	December 19, 2023 (submitted)
15	March 21, 2024 (revised)
16	Dateline

Submitted to Journal of Tropical Meteorology

Corresponding Author: Prof. Yuqing Wang, yuqing@hawaii.edu

18

17

1

20 Abstract

21

22

23

24

25

26

27

28

29

30

31

32

33

34

35

36

37

38

39

40

41

42

43

44

45

46

47

48

This study investigates the effect of the initial tropical cyclone (TC) vortex structure on the intensity change during the eyewall replacement cycle (ERC) of TCs based on two idealized simulations using the Weather Research and Forecasting (WRF) model. Results show that an initially smaller TC with weaker outer winds experienced a much more drastic intensity change during the ERC than an initially larger TC with stronger outer winds. It is found that an initially larger TC vortex with stronger outer winds favored the development of more active spiral rainbands outside the outer eyewall, which slowed down the contraction and intensification of the outer eyewall and thus prolonged the duration of the concentric eyewall and slow intensity evolution. In contrast, the initially smaller TC with weaker outer winds corresponded to higher inertial stability in the inner core and weaker inertial stability but stronger filamentation outside the outer eyewall. These led to stronger boundary layer inflow, stronger updraft and convection in the outer eyewall, and suppressed convective activity outside the outer eyewall. These resulted in the rapid weakening during the formation of the outer eyewall followed by a rapid re-intensification of the TC during the ERC. Our study demonstrates that accurate initialization of the TC structure in numerical models is crucial for predicting changes in TC intensity during the ERC. Additionally, monitoring the activity of spiral rainbands outside the outer eyewall can help to improve short-term intensity forecasts for TCs experiencing ERCs.

Key words: Tropical cyclones, concentric eyewall, inner eyewall and outer eyewall replacement cycle, intensity change,

1. introduction

The concentric (or double) eyewall structure is a common feature in strong tropical cyclones (TCs), which is characterized by the co-existence of the inner (primary) eyewall and the outer (secondary) eyewall. During the secondary eyewall formation (SEF) and the subsequent eyewall replacement, the TC intensity often experiences a first weakening and then a re-intensification. Namely, as the secondary eyewall forms and intensifies, the TC weakens, while when the outer eyewall continues to intensify and contract inward, the inner eyewall weakens and eventually is replaced by the outer eyewall, and the TC often re-intensifies (Willoughby et al. [1]; Houze et al. [2]). The subsidence over the inner eyewall forced by

convective heating in the outer eyewall and the blocking effect on the radial inflow by the outer eyewall are suggested to be responsible for the weakening and dissipation of the inner eyewall, leading to the significant weakening followed by re-intensification of the TC as the outer eyewall intensifies and contracts inward. However, although the overall structure and intensity change is well known, to what extent and what factors determine the intensity change are not fully understood (Wang and Wu ^[3]; Zhou et al. ^[4]; Wang ^[5]). As a result, large errors exist for TC intensity forecasts when TCs experience the SEF and the subsequent eyewall replacement (Sitkowski et al. ^[6]), or generally termed the eyewall replacement cycle (ERC).

Based on observations, Sitkowski et al. ^[6] indicated that most TCs experiencing ERCs possess three intensity change phases: intensification, weakening, and re-intensification. On average, the maximum tangential wind speed at 700 mb drops by 10 m s⁻¹ during the weakening phase. However, significant differences in duration and intensity change exist among different ERC cases. Based on the flight observational data, Willoughby and Shoreibah ^[1] found that during the ERC, the maximum tangential wind speed of Hurricane "Allen" (1980) changed by 25 m s⁻¹. The maximum wind speed of Typhoon "Sarah" (1956) decreased from 90 m s⁻¹ to 44 m s⁻¹. However, Zhou et al. ^[4] found that some ERC cases showed only a small decrease or even an increase in intensity after the SEF, such as Typhoons Pudal (2001), Dujuan (2003), and Lupit (2003). Kuo et al. ^[7] examined the intensity changes of concentric eyewall TCs over the western North Pacific during 1997–2006 and found that 71% of cases showed a decrease in intensity, while approximately 29% showed an increase within 24 h after the SEF. They also found that the intensity of weak (Categories 2 and 3) concentric eyewall typhoons decreased slower than that of strong typhoons (categories 4 and 5).

Many numerical modeling studies have also revealed various structure and intensity changes during the ERCs. Zhu et al. ^[8] found a rapid intensity decrease by 17 m s⁻¹ from nearly 60 m s⁻¹ to around 43 m s⁻¹ during the SEF in the simulated Hurricane Bonnie (1998). Zhu and Zhu ^[9] showed a 22 m s⁻¹ decrease in the maximum mean tangential wind at 1 km height in an idealized simulation of an SEF. In their numerical simulations, Tsujino et al. ^[10] studied the simulated Typhoon Bolaven (2012), whose intensity only slightly changed in 18 h after the SEF, which was attributed to the response of the inner eyewall to the blocking of high equivalent potential temperature and angular momentum transported into the inner eyewall. Zhu et al. ^[8]

indicated that the blocking effect of the outer eyewall became obvious when the outer eyewall intensified with increasing radial inflow and evolved into a quasi-axisymmetric structure. Bell et al. [11] found that the maximum near-surface wind speed of Hurricane "Rita" (2005) decreased abruptly after the SEF, primarily due to the decrease in radial inflow in the moat region. Namely, the radial outflow in the moat area induced by the intensifying outer eyewall convection blocked the radial inflow into the inner eyewall, causing the TC weakening. They also demonstrated that the subsidence forced by convective heating in the outer eyewall suppresses inner eyewall and contributed to the inner eyewall decay.

79

80

81

82

83

84

85

86

87

88

89

90

91

92

93

94

95

96

97

98

99

100

101

102

103

104

105

106

107

108

Zhou and Wang [12] proposed that the intensity change during ERC could be related to the width of the moat. They showed that the maximum wind speed in a sensitivity experiment with enhanced ice concentrations decreased by 12 m s⁻¹, while that in the control experiment decreased by only 5 m s⁻¹. They found that with the enhanced ice concentration the secondary eyewall formed in a larger radius and the time required for the eyewall replacement prolonged, leading to a larger weakening of the TC. As a result, the narrower moat in their control experiment corresponding to the shorter weakening time and thus smaller weakening in TC intensity during the ERC. Zhou et al. [4] compared concentric eyewall structures in TCs with and without large intensity weakening using the Tropical Rainfall Measuring Mission (TRMM) data and found that TCs with the outer eyewalls dominated by stratiform precipitation often had a more marked weakening than those dominated by convective precipitation. The latter often experienced insignificant weakening or even intensification. Results from numerical sensitivity experiments further indicated that the prevailing stratiform precipitation in the outer eyewall resulted in low equivalent potential temperature air in the moat area due to downdrafts and reduced the entropy of the boundary layer inflow to the inner eyewall, leading to a large TC weakening. Lai et al. [13] proposed that the barotropic instability might play an important role in the dissipation of the inner eyewall. The actual maximum surface wind speed of Hurricane "Wilma" (2005) dropped by around 15 m s⁻¹, which was simulated to drop by nearly 20 m s⁻¹.

Previous studies have mainly focused on the mechanisms of the SEF and TC intensity change during the ERCs. Some studies have identified several factors that may contribute to the difference in intensity change associated with the ERCs, such as the width of the moat, characteristics of precipitation in the outer eyewall, the barotropic instability of the moat, and

air-sea interactions. However, because of the complexity of TC intensity change induced by the ERCs, further understanding on the factors and processes that lead to large difference in TC intensity change during the ERCs are still required. Although some previous studies indicated the importance of the initial TC vortex structure to the timing of the SEF [14, 15], few studies have carefully examined the dependence of the intensity change during the ERC on the initial TC vortex. This study focuses on the possible effects of the TC structural differences on intensity change during the ERC based on idealized numerical simulations. The rest of the paper is organized as follows. The model description and experimental design are given in section 2. Section 3 presents the intensity and structure changes during the simulated ERCs. The relevant dynamic and thermodynamic processes are analyzed in section 4. The main results are summarized in the last section.

2. Model and experimental design

Two idealized numerical simulations of TCs with ERCs were conducted with the fully compressible, nonhydrostatic Weather and Research Forecasting (WRF) model version 4.3.1 (Skamarock et al. [16]). The model domain was triply nested, with the horizontal spacings of 18, 6, 2 km and the mesh sizes of 501×361, 361×361, 325×325. The model had 54 levels in the vertical direction with a mass vertical coordinate. The vortex–following technique was only applied in the innermost domain, which was initially located at the center of the middle and outermost domains. The model physical parameterizations included the Thompson scheme for cloud microphysics (Thompson et al. ^{17,18}), the Monin-Obukhov (Janjic) scheme (Monin and Obukhov [19]; Janjic [20]) for surface flux calculations, the Mellor-Yamada-Janjic (Eta) TKE scheme (Janjic [21]) for planetary boundary layer mixing. The modified Tiedtke cumulus parameterization scheme (Tiedtke, [22]; Zhang et al. [23]) was adopted in the outermost mesh only. The longwave and shortwave radiations were not considered in all simulations.

The unperturbed temperature and humidity profiles of the model atmosphere were those given by Dunion ^[24]. The model was initialized with an axisymmetric cyclone vortex similar to that used in Wang and Li ^[25]. The initial radial profile of tangential wind was given below:

$$V(r) = \begin{cases} V_m \frac{r}{r_m} \langle exp\left\{\frac{1}{b}\left[1 - \left(\frac{r}{r_m}\right)^b\right]\right\} - \frac{|r - r_m|}{R_0 - r_m} exp\left\{\frac{1}{b}\left[1 - \left(\frac{R_0}{r_m}\right)^b\right]\right\}\right\rangle, & r < R_0, \\ 0, & r \ge R_0 \end{cases}$$
(1)

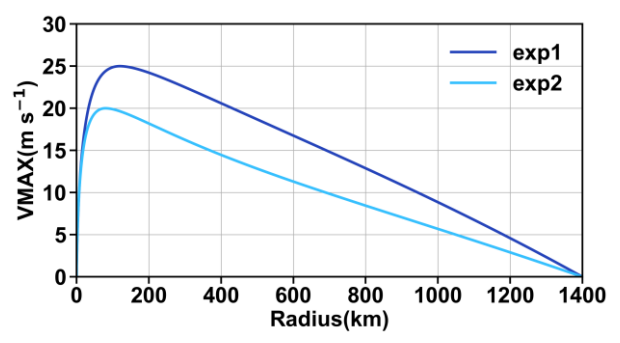


FIG. 1. The radial profiles of tangential wind (m s⁻¹) of the initial TC vortices used in exp1 and in exp2, respectively.

Two numerical experiments (exp1 and exp2) were performed with different initial parameters in the radial profile of tangential wind (Fig. 1). The maximum tangential wind speed of the initial vortex in exp1 was 25 m s⁻¹ at the radius of 120 km, and that in exp2 was 20 m s⁻¹ at the radius of 80 km. The initial tangential wind decreased radially to zero at the radius of 1400 km in both experiments and decreased linearly with height to zero at a height of about 18 km in both experiments. The parameter "b" was 0.3, and an *f*-plane at 18°N and a uniform SST of 28°C were assumed in both experiments. The different maximum wind speeds at different radii of the initial vortices in the two experiments were attempted to obtain the simulated TCs with different structural and intensity evolutions during their ERCs while with similar stead-state intensities with the same model configurations and the use of the same physical parameterizations in the simulations.

3. An overview of the simulated TC structure and intensity evolutions

We first provide an overview of the simulated eyewall cycles in the two simulations described in section 2. Both TCs experienced typical ERCs although considerable differences exist in details. Figure 2 shows the time evolution of the maximum wind speed at 10-m height and the corresponding radius of maximum wind (RMW) in the two experiments. We can see several distinct differences between exp1 and exp2 from Fig. 2. First, the SEF occurred after 73 h of the simulation in exp1 while after 100 h of the simulation in exp2. Here, the SEF (the gray horizontal solid lines in Fig. 2) is defined as the azimuthal mean upward vertical motion at 3 km height in the SEF region reached a value of 0.5 m s⁻¹ as in previous studies (e.g., Qiu and Tan [26]; Wang et al. [27, 28]). Note that the timing of the defined SEF here also corresponds to the appearance of the secondary maximum wind speed in the boundary layer (not shown).

The earlier SEF in the initially larger TC is consistent with a previous study ^[15]. Second, the intensity change during the ERC is considerably rapid in exp2 than in exp1 (see further quantification below). Third, the RMW is larger in exp1 than in exp2, consistent with the initially larger RMW in exp1 both before and after the ERC. Fourth, the RMW in exp1 displaces a larger fluctuation after the completion of the ERC and shows a consistent contraction much later than that in exp2. These differences indicate the crucial effects of the initial TC vortex structure and intensity to the simulated TC evolution and ERC. It is our interest in this study to find the key factors/processes that are responsible for the different intensity changes during the ERC between exp1 and exp2.

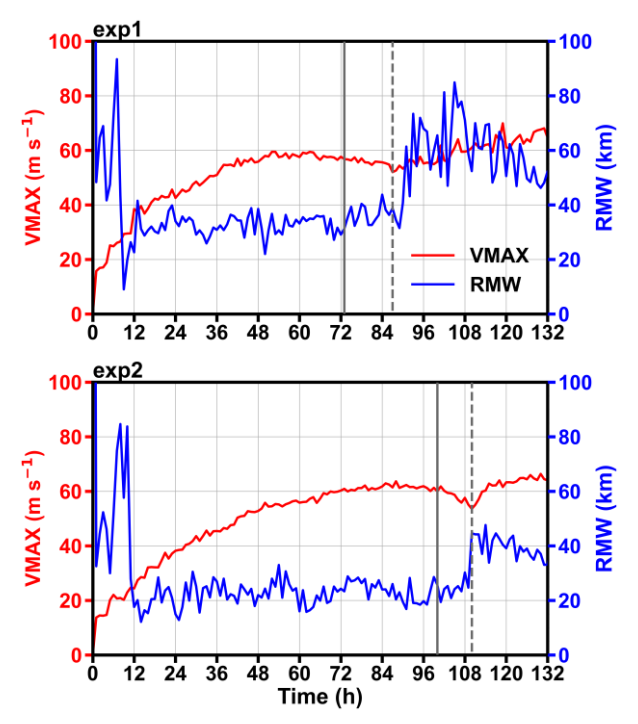


FIG. 2. Time evolution of the maximum 10-m wind speed (VMAX, m s⁻¹, red and left ordinate) and the radius of maximum wind (RMW, km, blue and right ordinate)

To facilitate our discussion, we reassign the time at which the secondary eyewall formed to 0 h as the new reference time for easy comparison of the two experiments. Figure 3 shows the time-radius Hovmöller diagram of the azimuthal mean vertical motion at 3-km and tangential wind speed at 1.5-km height in exp1 and exp2, respectively. We also show the time at which the simulated TC reached their minimum intensity (horizontal dash lines in Fig. 3) during the ERC in the corresponding experiments. Prior to the SEF, the radius of the maximum tangential wind (RMTW) at 1.5 km and the maximum eyewall updrafts are almost overlapped in both experiments, except for that the RMTW in exp1 is larger than that in exp2, suggesting

that the simulated TC inner-core size had some memory of its initial radius of maximum wind (RMW), consistent with a previous study of Xu and Wang ^[29]. In exp1 (Fig. 3a), the azimuthal mean upward motion near the radius of 80 km corresponds to the activity of inner spiral rainbands, while the scattered upward motions appearing beyond a radius of 150 km are related to the activity of outer spiral rainbands. As the outer spiral rainband contracted inward and intensified, a seemingly merging occurred with the original inner spiral rainbands, leading to the SEF near the radius of 90 km in exp1. As the outer eyewall continued contracting and intensifying, the inner eyewall weakened gradually and eventually replaced by the outer eyewall shortly after the TC reached its minimum intensity.

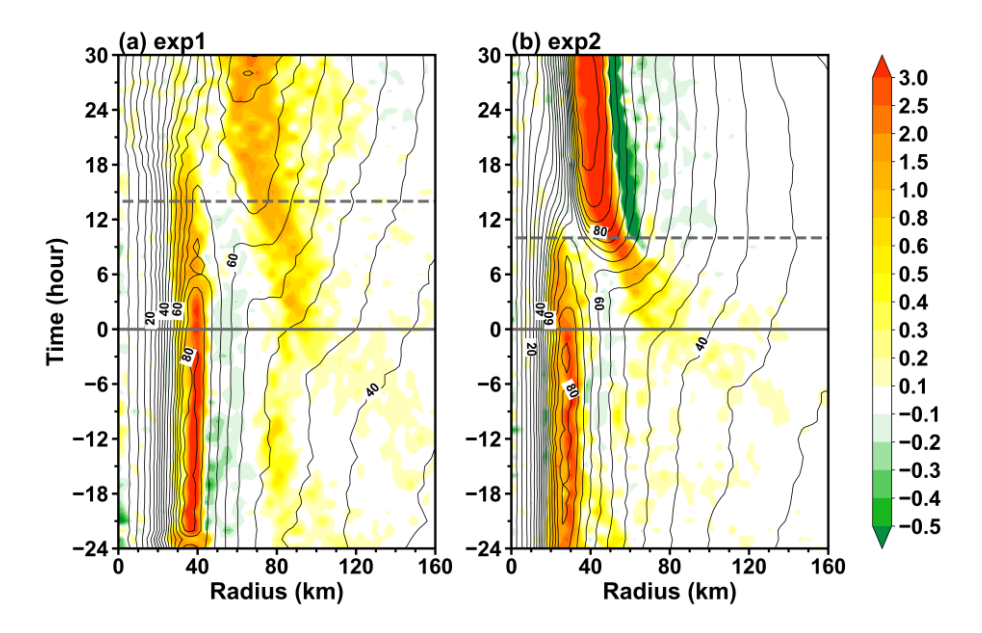


FIG. 3. Time-radius Hovmöller diagram of the azimuthal mean vertical motion at 3-km (color shades, m s⁻¹) and tangential wind speed at 1.5-km height (black contours, with contour interval of 5 m s⁻¹) in exp1 and exp2, respectively. The solid gray horizontal line highlights the time of the SEF, and the gray horizontal dashed line indicates the moment of minimum intensity during the ERC in the corresponding experiment.

The process in exp2 shows some differences (Fig. 3b). Due to the weak winds outside the RMW as shown in Fig. 1, upward motions beyond a radius of 60 km are less vigorous than in exp1, even up to 12 hours prior to the SEF. However, spiral rainbands developed around the radius of 140 km and became active afterward, leading to the SEF as the outer spiral rainbands contracted inward. The outer eyewall formed at about 80-km radius, which is slightly closer to the inner eyewall than in exp1. Interestingly, due to the smaller RMWs, the moat width in exp2 is similar to that in exp1. Because of the weak winds outside the RMTW (Fig. 1), the azimuthal mean upward motions outside the radius of 60 km are less active than those in exp1, even up to

12 h prior to the SEF. However, spiral rainbands developed around the radius of 140 km and became active afterwards, leading to the SEF as the outer spiral rainbands contracted inward. The outer eyewall formed at about 80-km radius, which is slightly closer to the inner eyewall than that in exp1. Interestingly, because of the smaller RMTW, the moat width in exp2 is similar to that in exp1. The duration of the concentric eyewall structure in exp2 was much shorter than that in exp1. The concentric eyewall structure in the latter maintained for only about 10 hours while that in the former maintained for about 18 h in terms of both the azimuthal mean vertical motion and the local maximum in the azimuthal mean tangential wind speed (Fig. 3). Another distinct feature is that vertical motion in the outer eyewall continued enhancing as the inner eyewall weakened and dissipated in exp2, while that in exp1 was considerably weaker but occurred in a much wider annular area in the outer eyewall than that in the inner eyewall prior to the SEF. In addition, we can see from the evolution of the azimuthal mean tangential wind speed in Fig. 3 that the intensity change was much drastic in exp2 than in exp1, which can be seen more clearly in Fig. 4, which depicts the time evolutions of the TC intensity in terms of maximum 10-m wind speed (VMAX) during the ERC in the two experiments.

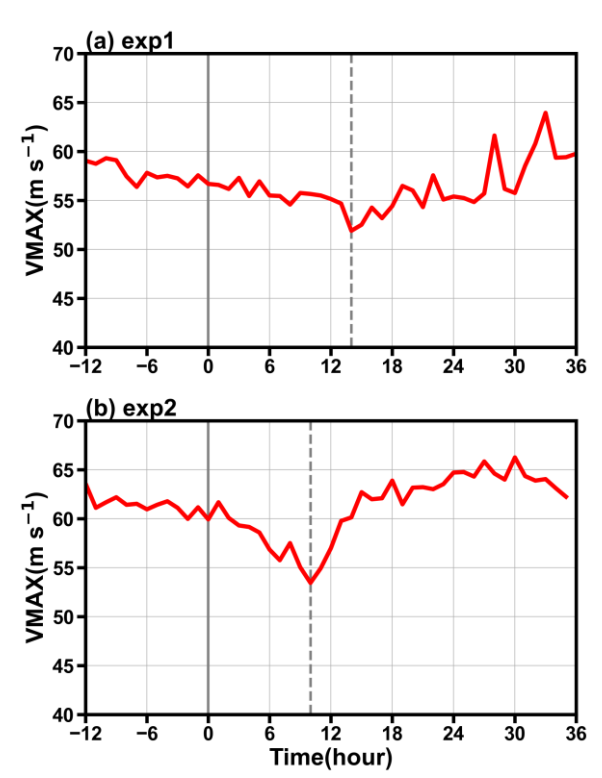


FIG. 4. Time evolutions of maximum 10-m wind speed in (a) exp1 and (b) exp2, respectively. The solid gray line highlights the starting time of the SEF, and the gray dotted line indicates the moment of minimum intensity when the time is reassigned as 0 h.

Both storms experienced ERCs but showed quite different intensity evolutions. In exp1 (Fig. 4a), the TC reached its peak intensity of 59 m s⁻¹ about 9 hours prior to the SEF, followed by a gradual weakening in response to active rainbands and the formation of the secondary eyewall. During 0-13 h, The VMAX dropped at a rate of -0.36 m s⁻¹ h⁻¹ from 56.7 m s⁻¹ to 52 m s⁻¹. Subsequently, the TC re-intensified slowly as the outer eyewall continued intensifying. In exp2 (Fig. 4b), after reaching a slightly higher peak intensity (63 m s⁻¹) to that in exp1, the VMAX remained stable at around 62 m s⁻¹ and was 60 m s⁻¹ at 0 h when the secondary eyewall formed. The VMAX dropped by 6.5 m s⁻¹ to 53.5 m s⁻¹ about 10 h later, with a weakening rate of -0.65 m s⁻¹ h⁻¹. This was followed by a rapid re-intensification for about 6 hours, and then a slow intensity evolution occurred afterwards. Compared the intensity change during the ERC between the two experiments, we can find that the two TCs had similar intensities prior to the SEF, but that in exp2 with a smaller and weaker initial TC vortex experienced more large intensity variation than that in exp1 while with a shorter period of concentric eyewall structure. These differences are related to convective activities in rainbands outside the outer eyewall after the SEF, which is primary due to the different initial vortex structures in the two experiments. Since the moat widths in the two experiments were similar as discussed above (Fig. 3), the moat width seems not to be the main reason for the different intensity changes between the two simulated TCs, previously noticed by Zhou et al. [4]. Our results suggest that the initially strong winds outside the RMW in the TC vortex in exp1 played some roles in suppressing any rapid intensity change during the ERC, which will be discussed in more detail in the next section.

4. Processes leading to the different intensity change during the ERC

223

224

225

226

227

228

229

230

231

232

233

234

235

236

237

238

239

240

241

242

243

244

245

246

247

248

249

250

251

It is our interest to examine the main processes that led to the different intensity changes during the ERC in the two experiments discussed in section 3. As we mentioned above, the moat width seems not to be the primary factor that can explain the difference in intensity change between exp1 and exp2. A distinct difference in the two experiments is the activity of spiral rainbands, as inferred from the azimuthal mean vertical motions at 3 km shown in Fig. 3. Therefore, our analysis will focus on the differences in the activity of spiral rainbands and their possible contributions to the different evolution in the simulated TC intensity during the ERC as shown in Fig. 4. For this purpose, we first examine the evolution of the plan view of radar

reflectivity at 3-km height, which can reflect the activity of spiral rainbands, in the two experiments given in Fig. 5. Both storms exhibited typical concentric eyewall structures with quasi-axisymmetric convective rings, but with different structure evolutions, which greatly contributed to the different intensity evolutions of the simulated ERCs between exp1 and exp2.

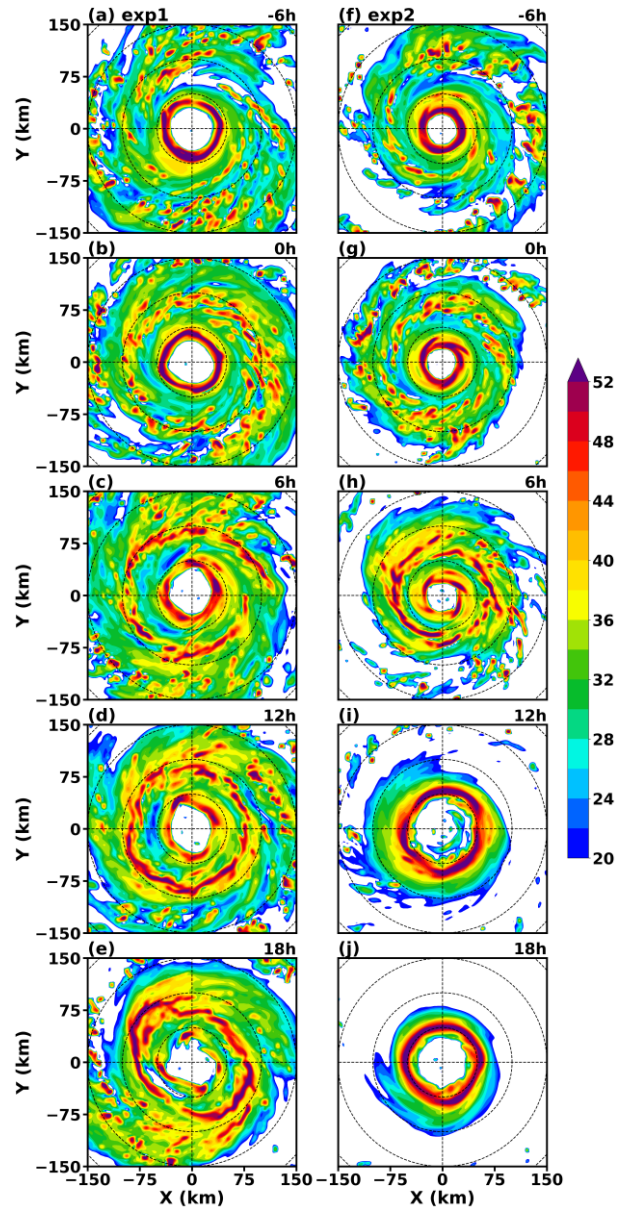


FIG. 5. Plan view of radar reflectivity (dBZ) at 3 km height in (a-e) exp1 and (f-j) exp2 from -6 h to 18 h at every 6 h interval, Concentric circles in each panel indicate the radii of 50, 100, and 150 km from the TC center at the given time in the corresponding experiments.

From Fig. 5, we can see that prior to the SEF, although spiral rainbands in exp1 were more active, with more inner and outer rainbands covering larger areas, than those in exp2 (Figs. 5a and 5f). During the period of the SEF, the intensity of the TC weakened gradually in both experiments. As the SEF approached, stronger convection appeared in the outer eyewall along

with more spiral rainbands outside the outer eyewall in exp1 (Fig. 5b) than in exp2 (Fig. 5g). The rainbands outside the outer eyewall in exp1 became more active by 6 h after the SEF and evolved into a predominant wavenumber-2 structure by 12-18 h after the SEF (Fig. 5c). As a result, a typical wavenumber-2 structure of the outer eyewall developed as the inner eyewall started weakening with the inner eyewall becoming polygonal and eventually dissipated (Figs. 5d, 5e). In sharp contrast, the rainbands outside the outer eyewall in exp2 were much less active than those in exp1. The outer eyewall contracted much faster and led to the completion of the ERC in only about 10 hours. This seems to strongly suggest that the activity of spiral rainbands outside the outer eyewall played a critical role in slowing down the inward contraction of the outer eyewall and thus elongated the duration of the concentric eyewall structure up to 18 hours in exp1. The consequence of this slow evolution also led to the less drastic intensity change in exp1 than in exp2.

To understand how the spiral rainbands outside the outer eyewall slowed down the outer eyewall contraction and contributed to the less drastic intensity change in exp1, we further compared in Fig. 6 the radius-height distributions of the azimuthal mean tangential wind and diabatic heating rate at the corresponding times as in Fig. 5 in exp1 and exp2. Consistent with what we see from Fig. 5, convective rainbands outside the outer eyewall in exp1 are more active and extended to larger radii (beyond 150 km) than those in exp2 prior to the SEF (Figs. 6a, 6f). Note that rainbands outside the outer eyewall in exp1 were more stratiform in larger radii as inferred by the relatively large diabatic heating rate above 5 km height at the time of the SEF as well as during the eyewall replacement (Figs. 6b–6e). Furthermore, the active rainbands in exp1 slowed down the post-ERC re-intensification of the simulated TC, which also led to a relatively weaker TC after the ERC than that in exp2 (Fig. 4).

The TC in exp2 showed more convective diabatic heating in both the inner and outer eyewalls, with much less active rainbands outside the outer eyewall during the ERC (Figs. 6g–6j). Convection in the new eyewall after the ERC was very strong with nearly axisymmetric convective ring structure and large diabatic heating rate. The new eyewall tilted radially outward with height, with diabatic cooling underneath, which was related to the melting of snow and graupel and evaporation of raindrops. The diabatic cooling with relatively strong subsidence under the titled eyewall convection suppressed convection outside the eyewall and

facilitating a rapid re-intensification and a higher intensity of the TC in exp2 (Fig. 4b). After the completion of the ERC, the TC showed a typical annular structure as defined by Knaff et al. [36] and numerically studied by Wang [31].

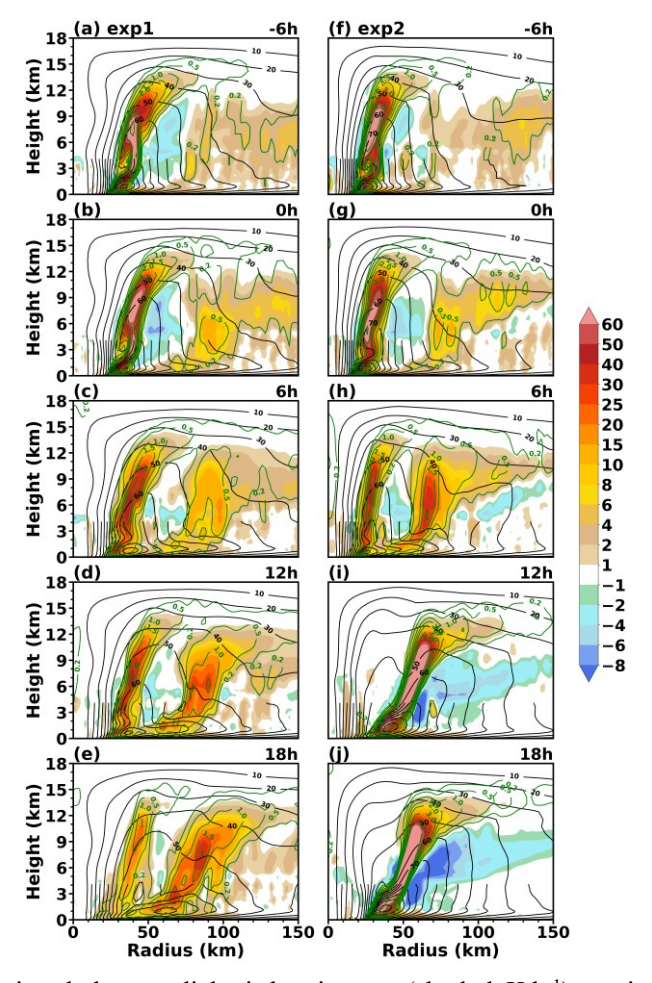


FIG. 6. Evolution of the azimuthal-mean diabatic heating rate (shaded; K h⁻¹), vertical motion (green contours at 0.2,0.5,1,1.5,2,3,4 m s⁻¹) and tangential wind (black contours with contour interval of 10 m s⁻¹, except below 4 km where the contour interval is 2 m s⁻¹) from -6 h to 18 h at every 6 h interval in (a-e) exp1 and (f-j) exp2.

The above analysis demonstrates that the existence of activity of spiral rainbands outside the outer eyewall is key to the intensity evolution during the ERC. The active rainbands outside the outer eyewall in exp1 played two important roles. On one hand, the transverse (secondary) circulation in response to diabatic heating in spiral rainbands outside the outer eyewall imposed a barrier effect on the inward penetration of boundary layer inflow toward the outer eyewall (Fig. 7), which was unfavorable for the contraction of the outer eyewall, contributing to the elongated duration of the concentric eyewall structure. On the other hand, the low-level inflow associated with diabatic heating in rainbands outside the outer eyewall played a role in spinning

up tangential winds outside the outer eyewall, favoring the outward expansion of the TC winds and increasing inertial stability outside the outer eyewall (Fig. 7). The relatively higher outer inertial stability would reduce the inflow response to the eyewall heating. This slowed down the re-intensification of the TC during the ERC in exp1. Note also that the broad wind of the initial TC vortex in exp1 implied relatively higher inertial stability outside the initial RMW, and thus partly contributed to the slower re-intensification of the TC, as discussed in previous studies with single eyewall TCs (Xu and Wang [32]; Li and Wang [33]).

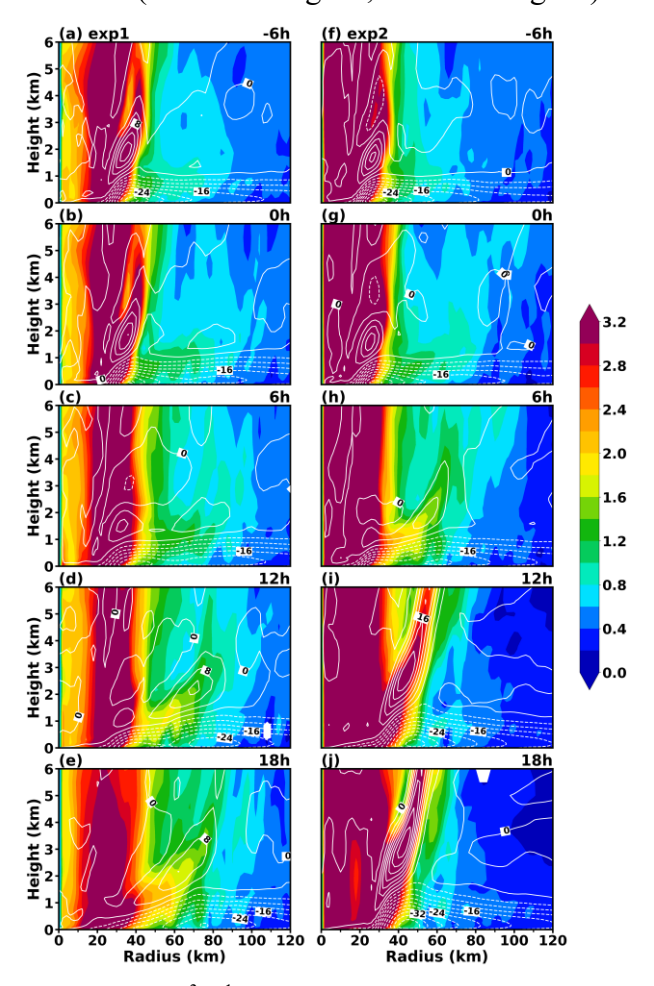


FIG. 7. The inertial stability (shaded; 10^{-3} s⁻¹) of the azimuthal mean TC vortex and the radial wind speed (contours, with interval of 4 m s⁻¹) in exp1 (a-e) and exp2 (f-j) from -6 h to 18 h at every 6-h interval. The inertial stability is defined $I = \sqrt{\left(f + \frac{2\bar{V}}{r}\right)\left(f + \frac{1}{r}\frac{\partial r\bar{V}}{\partial r}\right)}$, where \bar{V} is the azimuthal mean tangential wind speed.

Since the activity of rainbands outside the outer eyewall is key to both the duration of the ERC and the associated TC intensity change, a question arises as to why more active rainbands occurred in exp1 but less active in exp2. Since only difference between the two experiments in the experimental design was the use of different radial tangential wind profiles of the initial TC

vortices (Fig. 1), we thus can consider that the drastic difference in the activity of rainbands outside the outer eyewall between exp1 and exp2 should result primarily from the different radial wind profiles of the initial TC vortices. Indeed, previous studies have already extensively studied the dependence of the outward expansion of the tangential wind (size increase) and the TC intensification rate on the wind structure of the initial TC vortex (Xu and Wang [29, 32, 34]; Li and Wang [33]). For example, Xu and Wang [29] found that the simulated inner and outer core sizes increase was roughly proportional to the inner-core size of the initial TC vortex. They attributed such a relationship to the dependence of the simulated outer spiral rainbands on the radial tangential wind distribution of the initial TC. Namely, large winds outside the RMW in an initially large TC vortex favor strong sea surface enthalpy flux, which often facilitates convective activity and thus the activity of spiral rainbands, as also demonstrated in Xu and Wang [40]. This is because diabatic heating in outer spiral rainbands may result in broad lowlevel inflow and the spinning up of tangential wind outside the RMW, thus the increase in TC size. Xu and Wang [38] further found that an initially larger TC vortex would intensify more slowly than an initially smaller TC vortex due to relatively higher inertial stability and the more active outer spiral rainbands in the former than in the latter. In our simulations, the initial TC vortex in exp1 had a larger size with stronger winds outside the RMW than that in exp2 (Fig. 1). Therefore, more active rainbands outside the outer eyewall in exp1 resulted mainly from the initially broader wind distribution outside the RMW than in in exp2.

326

327

328

329

330

331

332

333

334

335

336

337

338

339

340

341

342

343

344

345

346

347

348

349

350

351

352

353

354

In addition to the effect on surface enthalpy flux discussed in previous studies, the radial distribution of tangential wind can also modify the so-called filamentation time (Rozoff et al. [35]), which can affect convective activity outside the RMW in a TC. Rozoff et al. [35] proposed that the sharp decrease in tangential wind outside the RMW corresponds to a strong stretching deformation area, which is termed the rapid filamentation zone (RFZ), within which convection is often suppressed. Since the initially different radial profiles of tangential wind in exp1 and exp2 given in (Fig. 1) also implies different filamentation time outside the RMW, it is our interest to analyze the filamentation time and its possible effect on the convective activity outside the outer eyewall during the ERC. Following Rozoff et al. [35], the filamentation time of the azimuthal mean TC vortex can be defined as

$$\tau_f = \left(-\frac{\bar{V}}{r}\frac{\partial \bar{V}}{\partial r}\right)^{-1/2},\tag{2}$$

356

357

358359

360361

362

363

364

365

366

367

368

369

370

371

372

373

374

375

376

377

378

379

380

381

where \bar{V} is the azimuthal mean tangential wind averaged in the 3-h period between 6–9 h after the SEF in each experiment.

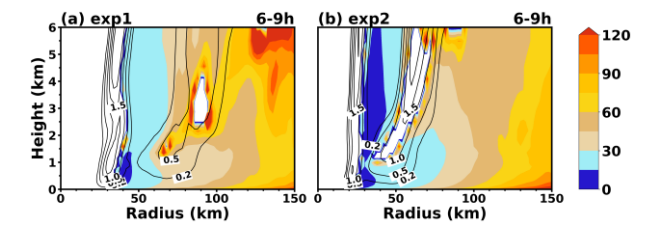


FIG. 8. Radius—height cross sections of the filamentation time (shaded; min) averaged in the 3-h period between 6–9 h after the SEF, and the black contours indicate the corresponding 3-h mean vertical motion with the contours of 0.2, 0.5, 1.0, 1.5, 2.0, 3.0, 4.0 m s⁻¹ in (a) exp1 and (b) exp2.

Figure 8 shows the radius-height distribution of the filamentation time of the simulated TCs in the two experiments based on model output at 6-min interval. It can be found that the moat area between the inner and outer eyewalls, as implied by strong upward motion, contours in Fig. 8, is characterized by the RFZ with filamentation time less than 30 min in both experiments. This is consistent with the findings of Rozoff et al. [35] and Wang [31]. Namely, rapid filamentation plays a role in suppressing convective activity in the moat area. However, the distribution of the filamentation time immediately outside the outer eyewall shows distinct differences between exp1 and exp2. Although the filamentation time is relatively short in the boundary layer under the outer eyewall in exp2, the area with the filamentation time outside the eyewall shorter than 45 min extends to a radius of 100 km and to a height up to 4 km (Fig. 8b). In contrast, the filamentation time outside the outer eyewall in expl is much longer. This indicates that convection outside the outer eyewall and thus the activity of spiral rainbands were not subject to strong filamentation in expl. This may explain why active spiral rainbands can survive outside the outer eyewall in exp1 (Figs. 5c, 5d). In contrast, strong filamentation outside the outer eyewall may play some roles in suppressing the activity of convective rainbands in exp2. Therefore, we can conclude that although larger enthalpy flux outside the outer eyewall due to larger near-surface winds facilitated active spiral rainbands in exp1, the overall weaker filamentation also favored convection and the activity of spiral rainbands. However, since the two processes co-exist, it is hard to quantify their relative importance to the simulated difference in rainband activity outside the outer eyewall between exp1 and exp2.

To further understand the dynamical processes leading to the different intensity evolutions during the ERC between exp1 and exp2, we performed an azimuthal mean tangential wind budget. The budget equation can be written below (Wang et al. [27]):

385
$$\frac{\partial \bar{v}}{\partial t} = -\bar{u}\overline{\zeta_{abs}} - \bar{w}\frac{\partial \bar{v}}{\partial z} - \overline{u'\zeta'_{abs}} - \overline{w'\frac{\partial v'}{\partial z}} + \bar{F_v}, \tag{3}$$

where t and z are time and height; \bar{v} , \bar{u} , \bar{w} , $\overline{\zeta_{abs}}$ and $\overline{F_v}$ are azimuthal mean tangential wind, radial wind, vertical velocity, absolute vertical vorticity, and vertical diffusion (including surface friction); v', u', w' and ζ'_{abs} are deviations of tangential wind, radial wind, vertical velocity, absolute vertical vorticity from their corresponding azimuthal means. The terms on the right-hand side of Eq. (3) represent the mean radial flux of absolute vertical vorticity or simply the mean radial advection (HADVm), mean vertical advection (VADVm), eddy radial flux of vertical vorticity or simply eddy radial advection (EHADV), eddy vertical advection (EVADV), and azimuthal mean diffusion (including surface friction, FRI). Note that the horizontal diffusion term is generally small during the ERC and is not included in our budget. To understand the intensity change during the ERC, we chose the 3-h period between 6-9 h after the SEF (note that results between 0-9 are similar). Our attention will be given to the weakening of the inner eyewall and intensification of the outer eyewall. The budget terms were calculated with the model output at 6-min interval. Our results indicate that the budgeted net azimuthal mean tangential wind tendency was consistent with the model simulated azimuthal mean tangential wind tendency (not shown). Therefore, the azimuthal mean tangential wind budget can be used to further understand the dynamical processes responsible for the different intensity changes simulated in exp1 and exp2.

Figures 9 and 10 show the budget results for exp1 and exp2, respectively. During the budget period, the TC intensity in exp1, which is still dominated by the intensity of the inner eyewall, did not show significant changes (Fig. 4a). The net tangential wind tendency in the inner eyewall shows little change in the near-surface layer and some positive values above (Fig. 9a). Some negative values in tangential wind tendencies appear in the eye region and the moat area. Weak but wide areas between 60–90 km are covered by positive tangential wind tendency below about 3-km height, indicating slow intensification of the outer eyewall. The mean radial advection contributes positively to the azimuthal mean tangential wind tendency in the

boundary layer and negatively immediately above due to the outflow layer associated with the upward advection of supergradient winds from the boundary layer in both the inner and outer eyewall updrafts (Fig. 9b, Li et al. [36]; Fei et al. [37]). The negative tangential wind tendency immediately above the boundary layer in the outwardly tilted eyewalls are largely offset by the positive tendency induced by vertical advection, which also partly offset the positive tangential wind tendency due to mean radial advection in the boundary layer (Fig. 9c). As a result, the net contribution by the mean radial and vertical advections to the azimuthal mean tangential wind tendency is positive in the boundary layer but negative immediately above the boundary layer (Fig. 9d). The positive tendency in the boundary layer contributed by the net mean radial and vertical advections is largely offset by the vertical diffusion and surface friction (Fig. 9e), while the negative tendency immediately above the boundary layer is partly offset by vertical diffusion. This suggests that the axisymmetric dynamical processes could not lead to the weak intensification of the outer eyewall and the eddy processes must play some important roles in expl. We can see from Figs. 9f-9h that although the eddy radial advection contributes negatively to the tangential wind tendency in the inner eyewall in the boundary layer, it contributes positively in the outer eyewall. The eddy radial advection causes negative azimuthal mean tangential wind tendency above the boundary layer (Fig. 9f), which is largely balanced by the eddy vertical advection (Fig. 9g). The eddy vertical advection contributes negatively to the intensification of the outer eyewall in the boundary layer, but positively above the boundary layer. Overall, the eddy processes contribute negatively in the middle boundary layer and positively in the lower boundary layer and above the boundary layer (Fig. 9h). The positive eddy contribution to the spinning up of the azimuthal mean tangential wind in the lower boundary layer in the outer eyewall region is consistent with that to the SEF previously documented by Wang et al. [27, 28]. Here, we found that the eddy processes partially offset the mean advective processes in intensifying the outer eyewall in the upper part of the boundary layer while contribute to the intensification of the outer eyewall immediately above the boundary layer.

411

412

413

414

415

416

417

418

419

420

421

422

423

424

425

426

427

428

429

430

431

432

433

434

435

436

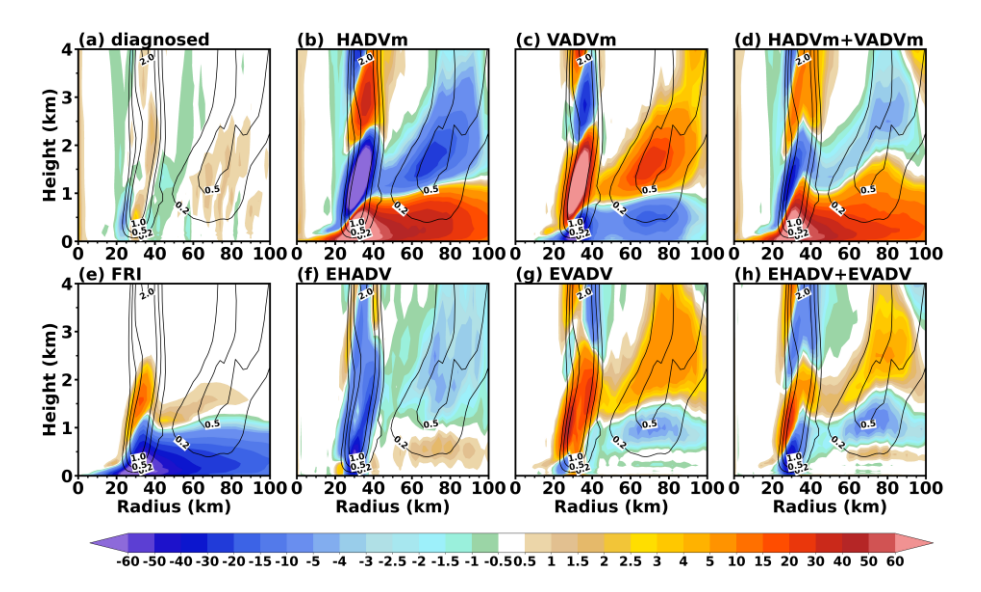


FIG. 9. The composite azimuthal-mean tangential wind budget (m s⁻¹ h⁻¹) over the 3-h period between 6–9 h after the SEF in exp1, (a) the net tangential wind tendency, (b) mean radial advection (HADVm), (c) mean vertical advection (VADVm), (d) the sum of (b) and (c) (HADVm+VADVm), (e) mean vertical diffusion and friction term (FRI), (f) eddy radial advection (EHADV), (g) eddy vertical advection (EVADV), and (h) the sum of (f) and (g) (EHADV+EVAD). The black contours indicate the 3-h averaged vertical motion with the contours of 0.2, 0.5, 1.0, 1.5, 2.0, 3.0, 4.0 m s⁻¹.

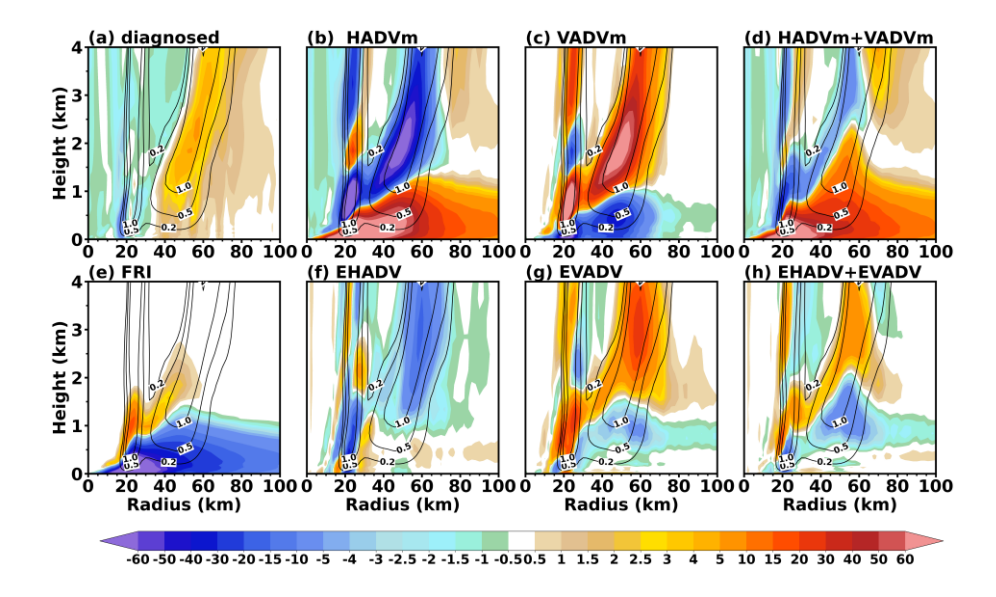


FIG. 10. As Fig. 9, but for the azimuthal mean tangential wind budget in exp2.

The azimuthal mean tangential wind budget in the same period for exp2 (Fig. 10) shows considerable differences from that in exp1. The net azimuthal mean tangential wind tendency shows considerable negative values in the inner eyewall but positive values in the outer eyewall, although the overall TC intensity only weakened slightly (Fig. 4b). This implies that the eyewall replacement occurred faster in exp2 than in exp1. The rapid weakening of the inner eyewall can

be simply attributed to the intensification of the outer eyewall, which acted as a barrier for the inward transport of both angular momentum and moisture into the inner eyewall. It is important to understand the dynamical processes that led to the rapid intensification of the outer eyewall and thus the rapid re-intensification of the storm in exp2 (Fig. 4b). Since the eddy processes in exp2 produced similar azimuthal mean tangential wind tendency as those in exp1 (Figs. 10f–10h), the larger positive tendency in the outer eyewall should be largely contributed by the mean advection processes (Fig. 10d). We can see from Figs. 10b–10d that the radial mean advection term shows much larger positive values in the outer eyewall region in the boundary layer in exp2 than in epx1 (Figs. 9b and 10b), and the mean vertical advection shows larger positive values in the outer eyewall above the boundary layer in exp2 than in exp1 (Figs. 9c and 10c). Note that the negative tendency near the inner edge of the outer eyewall above the boundary layer is compensated largely by the positive tendencies due to upward vertical mixing (Fig. 10e) and eddy vertical advection (Fig. 10g).

The larger contribution by the mean radial advection in the boundary layer in exp2 is due to higher inertial stability (and larger absolute vertical vorticity) and stronger inflow associated with the stronger secondary circulation induced by larger diabatic heating rate in the outer eyewall (Figs. 6 and 7). The higher inertial stability in the inner core was originated from the initially smaller inner-core size of the TC vortex, and the stronger inflow in the boundary layer was due to the lack of active spiral rainbands in exp2. These are consistent with the results discussed in Xu and Wang [32]. The higher winds of the initial TC vortex in exp1 acted in an opposite way by promoting more active spiral rainbands in the outer eyewall. Overall, the eddy processes associated with the convective activity in spiral rainbands outside and in the outer eyewall played a role in slowing down the intensification of the outer eyewall. Therefore, results from the azimuthal mean budget analysis further confirm that it is the difference in the radial wind profile of the initial TC vortex that determined the different intensity change of the simulated ERC in the two experiments.

5. Conclusions and discussion

Although previous studies have paid some attention to TC intensity change during the ERCs, the controlling factors and processes have not been well understood because of the

complexity of TC intensity change related to the ERCs. In this study, the WRF model was used to study the effect of initial TC vortex structure on the intensity change during the ERC of TCs. Two idealized simulations were conducted with the WRF model initialized with two TC vortices of different structures, one with a larger RMW and stronger intensity and one with a smaller RMW and weaker intensity. Although TCs in the two simulations developed concentric eyewall structures and experienced the ERC, their intensity evolutions behaved quite differently during the ERC. The TC initially with a larger vortex showed a very slow intensity evolution during the ERC and an elongated duration of the concentric eyewall structure, while the TC initially with a smaller vortex showed a drastic intensity change, namely a rapid weakening followed by a rapid re-intensification with a much shorter duration of the concentric eyewall structure.

By examining the intensity evolution and structural change, we discovered a close relationship between the difference in the activity of spiral rainbands outside the outer eyewall of the simulated TCs and the different intensity evolutions during the ERC. We observed that the TC initially with a larger RMW and high winds outside the RMW developed active spiral rainbands outside the outer eyewall during the ERC, while the TC initially with a smaller RMW and weak winds outside the RMW did not develop active spiral rainbands. Our study showed that the active spiral rainbands outside the outer eyewall played dual roles. On the one hand, the active rainbands reduced the inward penetrating inflow toward the outer eyewall, slowing down the contraction of the outer eyewall and elongating the duration of the concentric eyewall structure. On the other hand, active spiral rainbands played a role in slowing down the intensification of the outer eyewall by reducing the inward transport of angular momentum and moisture in the boundary layer (Wang [44]). As a result, active rainbands outside the outer eyewall in the TC initially with a larger RMW and high winds outside the RMW contributed to the slow intensity evolution and longer duration of the concentric eyewall structure. In contrast, the TC with less active spiral rainbands outside the outer eyewall after the SEF experienced a rapid weakening followed by a rapid re-intensification and a much faster completion of the ERC.

The difference in the activity of spiral rainbands outside the outer eyewall results primarily from the different structure of the initial TC vortices in the two experiments. Consistent with

previous findings (Xu and Wang ^[29]), higher winds outside the RMW in the initially larger RMW TC corresponded larger surface enthalpy flux, which facilitated the development of spiral rainbands outside the outer eyewall. We also found that weak winds outside the outer eyewall in the initially smaller RMW TC corresponded to the sharp decrease of tangential wind outside the outer eyewall, which would correspond to strong stretching deformation and rapid filamentation outside the outer eyewall, suppressing the development of convective rainbands. Therefore, the two processes related to the initial TC vortex structure played different roles in the two simulated ERCs, resulting in the difference in the activity of spiral rainbands outside the outer eyewall and thus the drastic difference in the intensity changes during the ERC of TCs and the duration of the concentric eyewall structure.

The azimuthal mean tangential wind budget analysis further revealed that was performed to understand the dynamical processes responsible for the different intensity changes in the two experiments. Results showed that relatively higher vertical vorticity (and thus higher inertial stability) outside the outside of the outer eyewall together with the eddy processes related to the activity of active spiral rainbands in the initially larger RMW TC vortex played an important role in slowing down the intensification of the outer eyewall. In contrast, the higher inertial stability in the inner core and weak inertial stability and strong filamentation outside the outer eyewall in the initially smaller TC vortex favored stronger inflow and eyewall convection but were unfavorable for active spiral rainbands, thus the large mean radial flux of absolute vorticity. These worked together to lead to the rapid intensification of the outer eyewall and thus the rapid weakening of the inner eyewall and the TC intensity and a rapid re-intensification of the TC in the later stage of the ERC.

We should point out that results from this study were based on idealized simulations. The intensity change during the ERC in real atmosphere could be more complicated. For example, the activity of spiral rainbands may also be affected by large-scale environmental flow, such as the vertical wind shear (e.g., Wang ^[5]). Note also that the activity of spiral rainbands is not only important for the intensity change during the ERC, but also key to the SEF. Our study could be valuable for enhancing our understanding of intensity change of TCs that develop a concentric eyewall structure. This is because we can monitor the activity of spiral rainbands outside the outer eyewall from satellite images. By analyzing the activity of rainbands outside the outer

- eyewall, we can estimate the duration and intensity change of the TC during the ERC. We are interested in exploring this possibility in our future work.
- 543 *Acknowledgments*: The authors thank two anonymous reviewers for their helpful review 544 comments. This study has been supported by National Natural Science Foundation of China
- under grants 41730960 and 41875057. YW was supported by NSF grant AGS-1834300.

REFERENCES

- 547 [1] WILLOUGHBY HE, CLOS JA, SHOREIBAH MG. Concentric eye walls, secondary wind maxima,
- and the evolution of the hurricane vortex [J]. Journal of the Atmospheric Sciences, 1982, 39: 395–
- 549 411, https://doi.org/10.1175/1520-0469(1982)039<0395:CEWSWM>2.0.CO;2.
- 550 [2] HOUZE R A, CHEN S S, SMULL B F, et al. Hurricane intensity and eyewall replacement [J]. Science,
- 551 2007, **315**: 1235–1239, https://doi.org/10.1126/science.1135650
- 552 [3] WANG Y Q, Wu C. Current understanding of tropical cyclone structure and intensity change
- s a review [J]. Meteorology and Atmospheric Physics, 2004, 87: 257–278, https://doi.org/
- 554 10.1007/s00703-003-0055-6.
- 555 [4] ZHOU X Q, WANG B, GE X Y, et al. Impact of secondary eyewall heating on tropical cyclone intensity
- change [J]. Journal of the Atmospheric Sciences, 2011, 68(3): 450-456, https://doi.org/
- 557 10.1175/2010JAS3624.1.
- 558 [5] WANG Y Q. Recent research progress on tropical cyclone structure and intensity [J]. Tropical Cyclone
- Research and Review, 2012, 1: 254–275, https://doi.org/10.6057/2012TCRR02.05
- [6] SITKOWSKI M, KOSSIN J P, ROZOFF C M. Intensity and structure changes during hurricane eyewall
- replacement cycles [J]. Monthly Weather Review, 2011, 139: 3829–3847, https://doi.org/10.1175/
- 562 MWR-D-11-00034.1
- 563 [7] KUO H C, CHANG C P, YANG Y T, et al. Western North Pacific typhoons with concentric eyewalls,
- Monthly Weather Review, 2009, 137: 3758–3770, https://doi.org/10.1175/2009MWR2850.1
- 565 [8] ZHU T, ZHANG D L, WANG F Z. Numerical simulation of Hurricane Bonnie (1998). Part I: Eyewall
- evolution and intensity changes [J]. Monthly Weather Review, 2004, 132, 225–241, https://doi.org/
- 567 10.1175/1520-0493(2004)132<0225:NSOHBP>2.0.CO;2
- 568 [9] ZHU Z D, ZHU P. The role of outer rainband convection in governing the eyewall replacement cycle
- in numerical simulations of tropical cyclones [J]. Journal of Geophysical Research-atmospheres,
- 570 2014, 119: 8049–8072, https://doi.org/10.1002/2014JD021899
- 571 [10] TSUJINO S, TSUBOKI K, KUO H C. Structure and maintenance mechanism of long-lived concentric
- 572 eyewalls associated with simulated Typhoon Bolaven (2012) [J]. Journal of the Atmospheric Sciences,
- 573 2017, 74: 3609–3634, https://doi.org/10.1175/JAS-D-16-0236.1
- 574 [11] BELL M M, MONTGOMERY M T, LEE W C, An axisymmetric view of concentric eyewall evolution
- in Hurricane Rita (2005) [J]. Journal of the Atmospheric Sciences, 2012, 69: 2414–2432,

- 576 https://doi.org/10.1175/JAS-D-11-0167.1
- 577 [12] ZHOU X Q, WANG B. Mechanism of concentric eyewall replacement cycles and associated intensity
- 578 change [J]. Journal of the Atmospheric Sciences, 2011, 68(5): 972–988, https://doi.org/10.1175/
- 579 2011JAS3575.1
- 580 [13] LAI T K, MENELAOU K, YAU M K. Barotropic instability across the moat and inner eyewall
- dissipation: a numerical study of Hurricane Wilma (2005) [J]. Journal of the Atmospheric Sciences,
- 582 2019, 76(4): 989-1013, https://doi.org/10.1175/JAS-D-18-0191.1
- 583 [14] ZHU Z D, ZHU P. Sensitivities of eyewall replacement cycle to model physics, vortex structure, and
- background winds in numerical simulations of tropical cyclones [J]. Journal of Geophysical
- 585 *Research: Atmospheres*, 2015, 120: 590–622, https://doi.org/10.1002/2014JD022056.
- 586 [15] GUAN L, GE X Y. How does tropical cyclone size affect the onset timing of second eyewall formation?
- 587 [J]. Journal of Meteorological Research, 2018, 32: 124–138, https://doi.org/10.1007/s13351-018-
- 588 7023-z
- 589 [16] SKAMAROCK W C, KLEMP J B, DUDHIA J, et al. A description of the Advanced Research WRF
- Version 3 (No. NCAR/TN-475+STR) [M]. University Corporation for Atmospheric Research, 2008: 1-
- 591 113, http://dx.doi.org/10.5065/D68S4MVH
- 592 [17] THOMPSON G, RASMUSSEN R M, MANNING K. Explicit forecasts of winter precipitation using
- an improved bulk microphysics scheme. Part I: Description and sensitivity analysis [J]. Monthly
- 594 Weather Review, 2004, 132: 519–542, https://doi.org/10.1175/1520-0493(2004)132
- 595 <0519:EFOWPU>2.0.CO;2
- 596 [18] THOMPSOPN G, FIELD P R, RASMUSSEN R M, et al. Explicit forecasts of winter precipitation
- using an improved bulk microphysics scheme. Part II: Implementation of a new snow
- 598 parameterization [J]. Monthly Weather Review, 2008, 136(12): 5095-5115, https://doi.org/10.1175/
- 599 2008MWR2387.1
- [19] MONIN A S, OBUKHOV A M. Basic laws of turbulent mixing in the atmosphere near the ground [J].
- Trudy Geofiz, Inst.AN SSR, 1954, 24: 1963–1987, https://api.semanticscholar.org/
- 602 CorpusID:198942767
- [20] JANJIC Z. The surface layer in the NCEP Eta Model. Eleventh Conference on Numerical Weather
- Prediction [C] // American Meteorological Society: 2006.
- 605 [21] JANJIC Z. The Step-Mountain Eta Coordinate Model: Further developments of the convection,

- viscous sublayer, and turbulence closure schemes [J]. Monthly Weather Review, 1994, 122: 927–945,
- 607 https://doi.org/10.1175/1520-0493(1994)122<0927:TSMECM>2.0.CO;2
- [22] TIEDTKE M. A comprehensive mass flux scheme for cumulus parameterization in large-scale models
- [J]. Monthly Weather Review, 1989, 117, 1779–1800, https://doi.org/10.1175/1520-
- 610 0493(1989)117<1779:ACMFSF>2.0.CO;2
- [23] ZHANG C X, WANG Y Q, HAMILTON K. Improved representation of boundary layer clouds over
- the Southeast Pacific in ARW-WRF using a modified Tiedtke cumulus parameterization scheme [J].
- Monthly Weather Review, 2011, 139(11): 3489-3513, https://doi.org/10.1175/MWR-D-10-05091.1
- 614 [24] DUNION J P. Rewriting the climatology of the tropical North Atlantic and Caribbean Sea atmosphere
- [J]. Journal of Climate, 2011, 24: 893–908, https://doi.org/10.1175/2010JCLI3496.1
- 616 [25] WANG B, Li X F. The beta drift of three-dimensional vortices: A numerical study [J]. Monthly
- 617 Weather Review, 1992, 120: 579–593, https://doi.org/10.1175/1520-0493(1992)120
- 618 <0579:TBDOTD>2.0.CO;2
- [26] QIU X, TAN Z M: The roles of asymmetric inflow forcing induced by outer rainbands in tropical
- 620 cyclone secondary eyewall formation [J]. Journal of the Atmospheric Sciences, 2013, 70: 953–974,
- 621 https://doi.org/10.1175/JAS-D-12-084.1
- 622 [27] WANG H, WU C C, WANG Y Q, Secondary eyewall formation in an idealized tropical cyclone
- simulation: balanced and unbalanced dynamics [J]. Journal of the Atmospheric Sciences, 2016, 73:
- 624 3911–3930, https://doi.org/10.1175/JAS-D-15-0146.1
- 625 [28] WANG, H, WANG Y Q, XU J, et al. The axisymmetric and asymmetric aspects of the secondary
- 626 eyewall formation in a numerically simulated tropical cyclone under idealized conditions on an f
- plane [J]. Journal of the Atmospheric Sciences, 2019, 76: 357–378, https://doi.org/10.1175/JAS-D-
- 628 18-0130.1
- 629 [29] XU J, WANG Y Q, Sensitivity of the simulated tropical cyclone inner-core size to the initial vortex
- 630 size [J]. Monthly Weather Review, 2010, 138: 4135–4157, https://doi.org/10.1175/2010MWR3335.1
- [30] KNAFF J A, KOSSIN J P, DEMARIA M. Annular hurricanes [J], Weather and Forecasting, 2003, 18:
- 632 204-223, https://doi.org/10.1175/1520-0434(2003)018<0204:ah>2.0.co;2
- [31] WANG Y Q. Rapid filamentation zone in a numerically simulated tropical cyclone [J]. Journal of the
- 634 Atmospheric Sciences, 2008, 65: 1158–1181, https://doi.org/10.1175/2007JAS2426.1
- 635 [32] XU J, WANG Y Q. Effect of the initial vortex structure on intensification of a numerically simulated

030	tropical cyclone [J]. Journal of the Meteorological Society of Japan, 2018, 96: 111–126, https://
637	doi.org/ 10.2151/jmsj.2018-014
638	[33] LI Y L, WANG Y Q, LIN Y L, et al. 2021: Why does rapid contraction of the radius of maximum
639	wind precede rapid intensification in tropical cyclones? [J]. Journal of the Atmospheric Sciences, 78:
640	3441-3453, https://doi.org/10.1175/JAS-D-21-0129.1
641	[34] XU J, WANG Y Q. Sensitivity of tropical cyclone inner core size and intensity to the radial distribution
642	of surface entropy flux [J]. Journal of the Atmospheric Sciences, 2010, 67: 1831-1852,
643	https://doi.org/10.1175/2010JAS3387.1
644	[35] ROZOFF C M, SCHBERT W H, MCNDLDY B D. Rapid filamentation zones in intense tropical
645	cyclones [J]. Journal of the Atmospheric Sciences, 2006, 63: 325-340, https://doi.org/10.1175/
646	JAS3595.1
647	[36] LI Y L, WANG Y Q, LIN Y L. 2020: How much does the upward advection of the supergradient
648	component of boundary layer wind contribute to tropical cyclone intensification and maximum
649	intensity? [J]. Journal of the Atmospheric Sciences, 2020, 77: 2649-2664, https://doi.org/10.1175/
650	JAS-D-19-0350.1
651	[37] FEI R, WANG Y Q, Li Y L. Contribution of vertical advection to supergradient wind in tropical
652	cyclone boundary layer: a numerical study [J]. Journal of the Atmospheric Sciences, 2021, 78: 1057-
653	1073, https://doi.org/10.1175/JAS-D-20-0075.1
654	[38] WANG Y Q. How do outer spiral rainbands affect tropical cyclone structure and intensity? [J]. Journal
655	of the Atmospheric Sciences, 2009, 66: 1250-1273, https://doi.org/10.1175/2008JAS2737.1